Title
Differential mitochondrial and cellular responses between H vs. J mtDNA haplogroup-containing human RPE transmitochondrial cybrid cells

Authors
Panvini, Ana Rubin
Gvritishvili, Anzor
Galvan, Hannah
et al.

Publication Date
2022-06-01

DOI
10.1016/j.exer.2022.109013

Peer reviewed

HHS Public Access

Author manuscript

Exp Eye Res. Author manuscript; available in PMC 2023 February 23.

Published in final edited form as:

Exp Eye Res. 2022 June ; 219: 109013. doi:10.1016/j.exer.2022.109013.

Differential mitochondrial and cellular responses between H vs. J mtDNA haplogroup-containing human RPE transmitochondrial cybrid cells

Ana Rubin Panvini[a,1], **Anzor Gvritishvili**[a,1], **Hannah Galvan**[a], **Sonali Nashine**[c], **Shari R. Atilano**[c], **M. Cristina Kenney**[c], **Joyce Tombran-Tink**[a,b,*]

[a] Department of Neural and Behavioral Sciences, Penn State College of Medicine, Hershey, PA, 17033, USA

[b] Department of Ophthalmology, Penn State College of Medicine, Hershey, PA, 17033, USA

[c] Department of Ophthalmology, Gavin Herbert Eye Institute, University of California Irvine, Irvine, CA, 92697, USA

Abstract

Mitochondrial dysfunction is associated with several retinal degenerative diseases including Age-related Macular Degeneration (AMD). Human mitochondrial DNA (mtDNA) haplogroups are inherited from a common ancestral clan and are defined by specific sets of genetic differences. The purpose of this study was to determine and compare the effects of mtDNA haplogroups H and J on transcriptome regulation and cellular resilience to oxidative stress in human RPE cytoplasmic hybrid (cybrid) cell lines in vitro.

ARPE-19 cybrid cell lines containing mtDNA haplogroups H and J were created by fusing platelets obtained from normal individuals containing H and J haplogroups with mitochondria-deficient (Rho0) ARPE-19 cell lines. These cybrids were exposed to oxidative stress using 300 μM hydrogen peroxide (H_2O_2), following which mitochondrial structural dynamics was studied at varying time points using the mitochondrial markers - TOMM20 (Translocase of Outer Mitochondrial Membrane 20) and Mitotracker. To evaluate mitochondrial function, levels of ROS, $\Delta\Psi m$ and $[Ca^{2+}]m$ were measured using flow cytometry, and ATP levels were measured using luminescence. The H and J cybrid cell transcriptomes were compared using RNAseq to determine how changes in mtDNA regulate gene expression. Inflammatory and angiogenic markers were measured using Luminex assay to understand how these mtDNAs influenced cellular response to oxidative stress. Actin filaments' morphology was examined using confocal microscopy.

Following exposure to H_2O_2 stress, the J cybrids showed increased mitochondrial swelling and perinuclear localization, disturbed fission and fusion, increased calcium uptake ($p < 0.05$), and higher secreted levels of TNF-α and VEGF ($p < 0.001$), compared to the H cybrids. Calcium uptake by J cybrids was reduced using an IP3R inhibitor. Thirteen genes involved in mitochondrial

* Corresponding author. Penn State College of Medicine, Hershey, PA, 17033, USA. jttink@aol.com, jxt57@psu.edu (J. Tombran-Tink).

[1] These authors contributed equally to this study.

Appendix A. Supplementary data

Supplementary data to this article can be found online at https://doi.org/10.1016/j.exer.2022.109013.

complex I and V function, fusion/fission events, cellular energy homeostasis, antioxidant defenses, and inflammatory responses, were significantly downregulated with log2 fold changes ranging between −1.5 and −5.1. Actin levels were also significantly reduced in stressed J cybrids ($p \leq 0.001$) and disruption in actin filaments was observed. Thirty-eight genes involved in mitochondrial and cellular support functions, were upregulated with log2 fold changes of +1.5 to +5.9 in J cybrids compared to H cybrids.

Our results demonstrate significant structural and functional differences between mtDNA haplogroups H vs. J-containing cybrid cells. Our study suggests that the J mtDNA haplogroup can alter the transcriptome to increase cellular susceptibility to stress and retinal degenerations.

Keywords

AMD; Age-related macular degeneration; Mitochondrial DNA haplogroups; mtDNA H haplogroup; mtDNA J haplogroup

1. Introduction

Mitochondria function as the primary regulators of cellular energy/ATP (Adenosine TriPhosphate) production via oxidative phosphorylation (OXPHOS), a process that generates reactive oxygen species (ROS) that can contribute to cellular oxidative damage (Ernster and Schatz, 1981). Mitochondrial DNA damage and dysfunction contributes to the development of aging-related retinal degenerative diseases such as Age-related Macular Degeneration (AMD), glaucoma, diabetic retinopathy, as well as other neurodegenerative diseases including Parkinson's disease, Alzheimer's disease, and Amyotrophic Lateral Sclerosis (Linnane et al., 1989; Lin and Beal, 2006; Schapira, 2008; Lustbader et al., 2004; Wong et al., 1995; Osborne, 2010; Kowluru and Chan, 2007; Shigenaga et al., 1994; Sastre et al., 2000; Wallace, 2005; Richter et al., 1988; Balaban et al., 2005; Wallace).

Mitochondrial DNA (mtDNA) is circular, double-stranded DNA that consists of 16,569 base pairs that code for 2 ribosomal RNAs, 22 transfer RNAs, and 13 polypeptides that constitute enzyme complexes of the OXPHOS pathway. The mitochondrial genes follow matrilineal inheritance, have high mutation rates due to lack of histones and inefficient DNA repair system, and can be grouped into haplogroups defined by single nucleotide polymorphisms (SNPs) (Wallace, 1994; Anderson et al., 1981; Van Oven and Kayser, 2009). These haplogroups include H, I, J, K, T, U, V, W, and X, which are most prevalent in European populations and have occurred over the last 75,000 years (Herrnstadt et al., 2002).

Previous studies have demonstrated that variations in mtDNA haplogroups are linked to an increased risk of disease development across populations. For example, the penetrance of Leber Hereditary Optic Neuropathy (LHON), a maternally inherited disorder caused by mutations in mtDNA, is higher in individuals with mtDNA haplogroup J background. Three primary LHON mtDNA mutations have been identified at nucleotide positions 3460, 11778, and 14484 and account for about 90% of world-wide LHON cases in the world. In these patients about 75% of the 14484 mutation was associated with the European mt haplotype J (Brown et al., 1997; Torroni et al., 1997; Hudson et al., 2007). Similarly, haplogroup J

has been shown to be a risk factor for AMD, while haplogroup H is considered to have a protective role in AMD. After adjusting for age, sex, and smoking, haplogroup H was shown to be associated with reduced prevalence of AMD at all stages of the disease, while J was associated with a higher prevalence of large, soft distinct drusen. When RPE cells containing J mtDNA were compared with those containing H mtDNA, J cells showed decreased expressions of high-risk genes for AMD including CFH, C3 and EFEMP1 (Kenney et al., 2013a, 2013b). Moreover, studies of cybrids containing J or H mtDNA haplogroups showed that J cybrids contain less mtDNA, RNA, and decreased oxygen consumption, mt membrane potential, and ATP production relative to H (Mueller et al., 2012; Jones et al., 2007). These observations have been attributed to reduced proton pumping activity in J mtDNA mitochondria, leading to lower oxygen consumption and less flow of electrons through the electron transport chain (ETC) within the mitochondrial inner membrane.

The goal of this study was to examine and compare the effects of mtDNA haplogroups H and J on transcriptome regulation and cellular resilience to oxidative stress in human RPE cytoplasmic hybrid (cybrid) cell lines in vitro.

2. Results

2.1. Morphological differences between H and J cybrids

Under normal growth conditions, three major morphological differences were observed between the H and J cybrids. Light microscopic analysis revealed that the H cybrids have greater cytoplasmic spreading compared to J cybrids. This was observed at the early stages (24 h–48 h) of cell seeding but less evident with increased confluency (~80%). Both H and J cybrid cells were examined 4 h after the addition of H_2O_2 and showed disruption of cell-cell adhesion and detachment from culture flasks after 4 h of exposure to oxidative stress. The second difference observed was in the structure and organization of the mitochondria. TOMM20 labeling indicated that these organelles consisted of highly interconnected and branched networks throughout the cytoplasm of H cybrids whereas they were structurally disconnected and localized to a perinuclear microdomain in the majority of J cybrids (Fig. 1). The third difference between the cells was seen in the structure of actin filaments shown by phalloidin staining. While actin filaments were distributed throughout the cytoplasm of H cybrids as well delineated bundles, they were less organized, showed evidence of depolymerization throughout the cytoplasmic compartment and were concentrated around the cytoplasmic edges of J cybrids (Fig. 1 and supplementary Figure 1).

2.2. Mitochondria and actin structure in J and H haplogroup mtDNA RPE cybrids under oxidative stress conditions

Mitochondria fusion dynamics in both cybrids were disrupted after exposure to oxidative stress. However, this was more severe in the J mtDNA haplogroup cells. In the J cells, these organelles were grossly swollen and disconnect from each other within an hour of oxidative stress. Actin filaments appeared depolymerized as well after brief (30 min) exposure to stress while these filaments remained relatively intact in H cells (Fig. 2 and supplementary Figure 2). Overall, H cybrids were more resistant to the effects of oxidative stress on the structural dynamics of both their mitochondria and actin components.

2.3. Mitochondrial calcium [Ca^{2+}]m uptake

We monitored dynamic changes in [Ca^{2+}]m uptake in the two RPE cybrid types in live cultures and observed that the [Ca^{2+}]m electrogenic process was not significantly different in the two cybrids under control non-stressed conditions. However, when the cells were exposed to oxidative stress for 0.5 h, J and H cybrids had a 4- and 2.8-fold increase in [Ca^{2+}]m uptake, respectively over their corresponding controls. [Ca^{2+}]m shifts were detected above control levels at 1 h of stress in the J and H cells, by 4.4 and 3.0-fold, respectively followed by a rapid decline in both cell types by 4 h (Fig. 3A).

2.4. Mitochondrial membrane potential (ΔΨm)

Similarly, the ΔΨm was not significantly different between the cybrids in non-stressed controls and there was little fluctuation in ΔΨm after stress insult for 0.5–1 h. However, there was a dramatic depolarization in both cybrids by 4 h of exposure to oxidative stress, the magnitude of which was ~2 fold more severe in J over the H cybrids (Fig. 3B).

2.5. Reactive oxygen species generation

Overall, ROS generation was 1.2-fold greater in H compared to J cybrids in non-stressed conditions. Both J and H cell types increased ROS production by ~1.2 fold over their respective controls at 0.5–1 h post stress conditions. Smaller increases in ROS production by 15.4% and 19.3% in J and H cybrids respectively were detected over controls at 1 h of stress. The greatest increase in ROS generation was seen in both cell types at the 4 h stress time point by 100% and 70% respectively in J and H from their baseline. The difference in ROS levels between the two groups at this time point were not statistically significant (Fig. 3C).

2.6. ATP levels

The production of ATP was markedly higher in H compared to J cybrids in stressed samples at all time points and even in control samples. There was 1.8-fold more ATP generated by H compared to J cells in control samples and the cells showed a rapid decline in ATP production by ~1.8 and ~2 fold, respectively after 0.5 h and by ~1.5 fold after 4 h exposure to oxidative stress compared to controls (Fig. 3D).

2.7. IP3R (Inositol TrisPhosphate Receptor) inhibition

Since calcium fluctuation was a major response of both J and H cybrids under stress conditions, we blocked the IP3R. Pre-treatment with the IP3Ri for 1 h prior to a 30 min exposure to stress resulted in a decreased [Ca^{2+}]m uptake by 2.6 and 1.6-fold in J and H cybrids, respectively, reaching values near baseline levels (Fig. 4). The observed effect was larger in magnitude in J cybrids compared to H. In addition to a reduction in [Ca^{2+}]m uptake in stressed cells after IP3R blockade, an unexpected finding was that mRNA levels of the IP3R and mitochondrial calcium uniporter (MCU), two calcium transporters, were both decreased in J cybrids compared to H by 1.6- and 1.5-fold, respectively, in control samples (Fig. 4). IP3R inhibition ameliorated effects of oxidative stress on mitochondrial fission, perinuclear location, and swelling in J cybrids (Fig. 5).

In summary, RPE cells containing the J haplogroup mtDNA generated less ATP and ROS in non-stressed conditions and responded to oxidative stress with rises in $[Ca^{2+}]m$ and decreased $\Delta\Psi m$ when compared to RPE cells containing H mtDNA. Blocking the IP3R calcium transporter reduced the effects of stress on mitochondrial fission/fusion dynamics, swelling and cytoplasmic distribution.

2.8. Global transcriptome analyses in H and J cybrids

The heatmap in Fig. 6 compares global transcriptome characteristics of H and J cells. The graph shows differentially expressed genes ranked by fold change. Thirteen genes were downregulated in J cybrids with log2 fold changes of − 1.5 to - 5.1 and thirty-eight upregulated with log 2-fold changes of +1.5 to +5.9. The top protein coding genes that were downregulated in J compared to H include MMP1, SEPP1, ALMS1, and MT-ATP8, with activities related to extracellular matrix homeostasis, oxidative stress protection and mitochondrial function. Upregulated protein coding genes that were upregulated in J compared to H cell types with the highest $\log_2$ fold changes include CKB and TXNIP with functional activities related to ATP phosphorylation and oxidative stress.

2.9. RT-qPCR validation

From the RNAseq analysis a group of seventeen mitochondrial genes that showed regulation differences between H and J cybrids were chosen for validation using PCR. The histogram in Fig. 7 represents RT and qPCR data that confirm fold change differences in J relative to H cybrids. Several mitochondrial fission and fusion genes including MFN1, MFN2, DRP1, FIS1, OPA1 and genes regulating mitochondria ATP levels including MT-ATP8 and MT-ATP6 were confirmed to be downregulated in J compared to H cybrids.

2.10. Analysis of IL-6, IFN- γ, MCP-1, TNF- α, and VEGF

J and H cells did not show a statistically significant difference in levels of IFN- γ and VEGF under control condition. However, J and H cybrids showed an increase in VEGF levels under stress by 15.7 and 3.6% respectively, and this difference was statistically significant ($p < 0.001$). On the other hand, levels of TNF- α and IL-6 were secreted at higher levels in H cells compared to J under control conditions ($p < 0.05$) and while TNF-α increased with stress by 65.1 and 25.6% over their controls in J and H cells, respectively, it was secreted at higher levels in J cybrids by 39.5% ($p < 0.001$); while IL-6 at lower levels by 6.2% ($p < 0.001$) over H cells in stress conditions (Fig. 8).

3. Discussion

The current study demonstrated that compared to H cybrids, the J cybrids showed increased actin filament disruption, mitochondrial dysfunction and reorganization, and downregulation of genes involved in mitochondrial function. The results presented in this paper are novel as this is for the first time that we have demonstrated the response of H and J cybrids to hydrogen peroxide, RNA sequencing, and validation using qPCR. Our previous paper compared the growth rate and complement genes between H vs. J cybrids (Malik et al., 2014a).

Compared to J cybrids, the H cybrids grow slower, have higher baseline ATP production, and they also generate higher levels of ROS. H and J cybrids differ in the expression of nuclear genes involved in inflammation and human retinal diseases. In our previous study, we expanded the analysis of cellular behavior into their ability to form monolayers and an extended analysis into energy metabolism. The H cybrids were found to develop better barrier function than the J cybrids, with transepithelial epithelial resistance values differing significantly by ~15%. The H cells have higher levels of OXPHOS, and glycolysis as measured by OCR (Oxygen Consumption Rate), a measure of cellular respiration rate and mitochondrial function, and also exhibit higher basal respiration and maximum respiration, with the coupling efficiency of the ECT being tighter, leading to a lower proton leak. The biggest difference between H and J cybrids was the reduced effect of shutting down complex V with oligomycin, suggesting impaired ATP synthase activity. ECAR (Extracellular Acidification Rate), a measure of glycolysis, measurements in response to oligomycin also suggest that the rate of glycolysis is significantly reduced in J cybrids when compared to H cybrids. Although the determinants of cell size remain elusive (Marshall et al., 2012), actin is known to play a role in cell shape, size, and mitochondrial motility (Cooper, 2000). This is seen in mutant Dictyostelium lacking two F-actin crosslinking proteins, α-actinin and gelation factor, which showed reduced cell size and increased sensitivity to osmotic stress (Rivero et al., 1996), and in studies showing that mutations in the actin gene ACT1 result in defects in mitochondrial distribution and motility in hippocampal neurons (Furukawa et al., 1995; Wang et al., 2002). Given the relationship between actin and mitochondrial mechanobiology, it is likely that the J mtDNA increased RPE cell susceptibility to stress by decreasing actin expression levels and inducing actin depolymerization, mechanisms that can influence mitochondrial cell spreading, motility and fission/fusion dynamics (Fehrenbacher et al., 2004; Moore et al., 2016; Morris and Hollenbeck, 1995; Boldogh and Pon, 2006).

The increased ATP and ROS levels in RPE cells containing H mtDNA is likely to reflect higher ETC efficiency, ATP synthase activity and energy production compared to cells with J haplogroup mtDNA. These findings are consistent with previous studies showing that J cybrids had increased levels of lactate, indicating a stronger reliance on glycolysis when compared to the OXPHOS efficient H cybrids (Kenney et al., 2013a). Only minor differences were noted in the mitochondrial membrane potential between the two cybrids under stress conditions suggesting that while J haplogroup mtDNA renders cells susceptible to small doses of stress it did not drive them towards an apoptotic pathway in our experimental paradigm.

Mitochondrial haplogroup types can also influence calcium (Ca^{2+}) regulation and signaling, but the implications of this observation have been limited by our current knowledge of the mitochondrial calcium transport systems (Kazuno et al., 2006, 2008). Calcium (Ca^{2+}) is a key signaling factor in ROS and energy generation. It stimulates ATP production by activating TCA dehydrogenases in the mitochondrial matrix (McCormack and Denton, 1994) and can promote cell death through necrosis and apoptosis (Pinton et al., 2008a). Mitochondrial-associated ER membranes (MAMs) are an important site of cellular Ca^{2+} regulation. They physically link the inositol 1,4,5-trisphosphate receptor (IP3R) in the ER with mitochondrial voltage-dependent anion channels (VDAC). This association facilitates

Ca^{2+} fluxes between the organelles. Aberrant mitochondria Ca^{2+} fluxes can alter normal mitochondrial function and modulate mitochondrial dynamics (Rivero et al., 1996; Brookes et al., 2004; Rizzuto et al., 2009; Malik et al., 2014b; Wilkins et al., 2014).

The complex dynamics between the ER, mitochondria, Ca^{2+} and ROS are not entirely understood. However, since mtDNA encodes essential components of the ETC, mitochondrial Ca^{2+} handling machinery and cell death processes, the role of mtDNA variations that disrupt these processes is relevant in the pathogenesis of many neurodegenerative diseases.

Inhibition of the inositol 1,4,5-trisphosphate receptor (IP3R) efficiently lowered the levels of mitochondrial calcium influx under stress conditions and had a protective effect on the structure and distribution of mitochondria, showing preservation of branching networks throughout the cytoplasm of J cybrids. Dysfunction of the IP3R has been linked to neurodegenerative disorders such as Alzheimer's disease, spinocerebellar ataxias, and Huntington's disease (Egorova and Bezprozvanny, 2018; Egorova et al., 2015; Hisatsune and Mikoshiba, 2017). Although cellular calcium dynamics are complex and not entirely understood, there is evidence that disruption of calcium signaling leads to neuronal cell death in transgenic mouse models (Bezprozvanny, 2011). To our knowledge, there are no reports on the role of IP3R dysfunction in the pathogenesis of AMD, and future studies are needed to further investigate this relationship and its potential therapeutic implications.

One of the key findings from our work is that J and H haplogroup mtDNA exert strong regulatory influence on the RPE transcriptome, implying that their respective mutations can control nuclear responses to the environment, in this case stress. A group of important genes controlling both mitochondrial and cellular functions showed differences in expression levels between the two cybrids. Two genes, MMP1 and SEPP1, showing the highest decrease in expression levels in J relative to H mtDNA cells, are relevant to neurodegenerative conditions (Kim and Joh, 2012). For example, matrix metalloproteinases (MMPs) are known to play a key role in hydrolyzing components of the extracellular matrix (ECM) and many, including MMP1, are localized to Bruch membrane (Nagase et al., 2006; Guo et al., 1999). A widely accepted theory is that abnormal ECM turnover contributes to Bruch's membrane pathology and the development of AMD (Zarbin, 2004). Our study suggests that in oxidative stress conditions, J haplogroup mtDNA may promote disruption of normal ECM remodeling in Bruch's membrane and contribute to AMD by reducing expression and secretion of MMP1 in the retina (Alge-Priglinger et al., 2009).

SEPP1, on the other hand, codes for selenoprotein P, which is implicated in antioxidant function. It protects neuronal cells from the neurotoxic effects of aggregated amyloid beta (Aβ) peptides (Takemoto et al., 2010) and prevents oxidative damage in human endothelial cells by restoring the enzymatic activity of glutathione peroxidase (Steinbrenner et al., 2006a). Selenoprotein P deficiency in human astrocytes increases susceptibility of the cells to oxidative stress-induced cytotoxicity (Steinbrenner et al., 2006b). Reduction in SEPP1 expression and its antioxidant function in J mtDNA RPE cells may underlie the mitochondrial dysfunction we observed in these cells under oxidative stress conditions.

Transcriptional changes in a group of mtDNA encoded genes which are important to the function of respiratory complexes I, IV and V of the ETC were also detected in RPE cells containing J mtDNA when compared to their H mtDNA counterpart. Expression levels of MT-ATP8, MT-ATP6 (Complex V), MT-ND3 (Complex I), and MT-CO3 (Complex IV) were among the top 10 genes showing decreased expression in J cybrids by RNAseq analysis results which were validated by both RT- and qPCR. This further supports the hypothesis that energy production in J mtDNA cybrids is less efficient and may increase the cell's susceptibility to oxidative damage.

Several nuclear-encoded genes associated with important mitochondrial function including MFN1, MFN2, DRP1, FIS1 and OPA1 were also downregulated in the J mtDNA cybrids. DRP1 regulates mitochondrial fission (Frank et al., 2001), while OPA1 and the mitofusins (MFN1, MFN2) play a critical role in inner and outer mitochondrial membrane fusion, respectively (Santel and Fuller, 2001; Olichon et al., 2002). The expression changes in this subset of nuclear-encoded genes undoubtedly influenced the structural and functional disturbances we observed in the mitochondria of the RPE J mtDNA cybrids.

It is interesting to note that the J mtDNA haplogroup, which as previously cited has a known association with AMD progression(Kenney et al., 2013a, 2013b; Mueller et al., 2012; Jones et al., 2007), also upregulated expression of many cytokines by RPE cybrids in stress conditions. Levels of inflammatory cytokines are of relevance in the pathogenesis of many neurodegenerative disorders including AMD. IFN-γ was found to be upregulated in J cyrbids compared to H cybrids and this is critical because IFN-γ contributes to the development of ocular inflammation and loss of retinal neurons (Geiger et al., 1994). Similarly, compared to the H cybrids, TNF-α protein was found to be significantly increased in J cybrids. Since the J haplogroup is high risk for AMD, our results support the results of previous studies which demonstrated TNF-α as a key contributor to AMD pathogenesis (Khan et al., 2021; Touhami et al., 2018). IL-6 is an inflammatory marker that is independently associated with the progression of AMD (Seddon et al., 2005) and VEGF has an important role in the development of choroidal neovascularization in this disease (Kvanta et al., 1996). The differential expression of inflammatory molecules by J and H cybrids under stress implicates their respective mtDNA in controlling the cell's inflammatory drive in pathological conditions. However, more studies are needed to further understand the relationship between variations in mtDNA and inflammation.

We would also like to acknowledge the limitations of this study. Since the goal of the study was to examine the role of H and J mitochondria in RPE cells, we used the immortalized ARPE-19 cell line as the parent cell line from which the nuclei of the transmitochondrial cybrids were derived. We could not use primary RPE cells that show transepithelial resistance and polarization because growing those cells is relatively difficult, labor-intensive, and time-consuming. In physiologic conditions in-vivo, RPE cells are highly differentiated with tight junctions, highly resistant to stress, form the outer blood-brain barrier, support photoreceptor cells, and enable transepithelial transport and phototransduction. The ARPE-19 cell line is a rapidly growing immortalized human cell line derived from primary RPE cells from the globes of a 19-year-old male donor. We have confirmed that our ARPE-cell lines express RPE cell-specific markers CRALBP and RPE65

and form a viable cuboidal to columnar epithelium monolayer in culture media (Hamid et al., 2021). Although ARPE-19 cells retain the characteristic features of RPE including defined cell borders and pigmentation, they require considerable time for differentiation and are unable to completely differentiate into RPE-like layers found *in vivo*. ARPE-19 cells show partial polarization as some of the cells in the monolayer resemble the morphology of differentiated RPE cells such as apical microvilli, polarized distribution of organelles, basolateral infoldings, and junctional complexes on the apical plasma membrane. ARPE-19 cells exhibit low transepithelial resistance (TER) that reaches a maximum value of 50–100 $\Omega\ cm^2$ after 28 days of culture in low-serum media in laminin-coated Transwell-COL filters. It is speculated that the low TER might be due to heterogeneity of the cell line since some of the cells show polarization. We acknowledge that a limitation of this study is that since ARPE-19 cells express CRALBP and RPE65 when grown appropriately as polarized monolayers, monolayers would have been preferable.

Intracellular calcium homeostasis regulates apoptotic cell death, and mitochondria is a critical check point in this process. Intracellular free calcium is essential for the maintenance of normal retinal function in RPE cells. Therefore, accurate control of calcium is vital in these cells. Because Ca^{2+} is permanently extruded from the cytosol, RPE cells need a basal Ca^{2+} entry pathway that counteracts this Ca^{2+} efflux. The TRPC channels that facilitate Ca^{2+} entry into the RPE cells contribute to the resting membrane potential and regulate basal regulatory processes such as secretion of cytokines in RPE cells. Trigger of RPE cell death depends on the transfer of calcium from the endoplasmic reticulum to the mitochondria, and abnormally high baseline Ca^{2+} level contributes to RPE degeneration in AMD (Wimmers and Strauss, 2007; Pinton et al., 2008b; Kaarniranta et al., 2020; Ishii and Rohrer, 2017). In summary, our study expands our current understanding of mitochondrial haplogroups, and shows that variation in types of mtDNA can influence nuclear decisions in transcriptome regulation, mitochondrial fusion/-fission dynamics and a cell's ability to cope with oxidative stress. These findings highlight the importance of J mtDNA as a key player in neurodegenerative disorders and conditions that primarily arise from oxidative damage.

4. Materials and methods

4.1. Culture of mitochondrial DNA cybrids

H and J mtDNA cybrids were generated using human ARPE19 cells (ATCC; Manassas, VA) and donor platelets as we have previously described (Hudson et al., 2007; Kenney et al., 2014a, 2014b). 10 mls of peripheral blood were collected via venipuncture in tubes containing 10 mM EDTA from normal volunteers having H and J mtDNA haplogroups. Platelets were isolated by a series of centrifugation steps and final pellets were suspended in Tris-buffered saline. The ARPE-19 cells deficient in mtDNA (Rho0) were created by serial passage in low dose ethidium bromide. Cybrids were produced by polyethylene glycol fusion of platelets with Rho0 ARPE-19 cells according to modified procedures of Chomyn. All experiments used passage 5 cybrid cells. The cell lines were cultured in Dulbecco's Modified Eagle Medium (DMEM-F12) (Corning/Cellgro; Manassas, VA) supplemented with 10% fetal bovine serum (FBS), 1% penicillin-streptomycin, 0.1% Gentamicin and 1% Fungizone at 37 °C with 5% CO2. Cells were seeded out at a density of 5×10^3 cells/ml

and grown to 80–90% confluency before experimental measurements were carried out. In oxidative stressed conditions, cultures with confluent monolayers were treated with 300 μM tert butyl hydrogen peroxide (H_2O_2) (Sigma Aldrich; St. Louis, MO) for 0.5–4 h in serum-free medium (SFM). All analyses below were carried out two times in triplicates (n = 6).

The cells were all grown to confluence and treated with hydrogen peroxide as monolayers for 0.5–4 h before lifting off for both Flow cytometry measurements and PCR. The H_2O_2 treated cells were then labeled with reagents to measure ROS, Calcium, membrane potential and ATP levels. All data were compared to controls treated exactly the same way. This was the most efficient way to do the experiments to avoid any interference of trypsin on the various dyes used for mitochondrial functional measurements and to also keep the incubation time of each dye exactly the same. The differences observed in the functional measurements were only due to oxidative stress after exposure of confluent monolayers cultures to H_2O_2.

4.2. Cell morphology

4.2.1. Immunocytochemistry (ICC)—Cells grown on glass coverslips were fixed for 1 h at room temperature (RT) using 4% paraformaldehyde (PFA) dissolved in phosphate buffered saline (PBS), washed, and then incubated for 30 min at RT in a PBS-based blocking buffer containing 0.3% Triton X-100, 5% bovine serum albumin. All antibodies used were diluted in this blocking buffer. Samples were subsequently incubated overnight at 4 °C with TOMM20 (1:200) rabbit polyclonal antibody (Catalog number - FL-145; C11415; Santa Cruz Biotechnology; Santa Cruz, CA), washed, and incubated with DyLight 488- conjugated AffiniPure Goat Anti-Rabbit IgG (1:400) (RRID: AB_2339507; Jackson ImmunoResearch Laboratories; West Grove, PA) for 1 h at RT. Coverslips were then stained with Texas Red-X phalloidin (1:70 in PBS) (Invitrogen Molecular Probes; Eugene, OR) for 30 min at RT, washed and then stained with Dapi (1:10,000 in PBS) for 5 min. Coverslips were mounted on slides using SlowFade Gold antifade (Invitrogen; Life Technology; Carlsbad, CA), fluorescence signals visualized by confocal microscopy (Fluoview FV1000 confocal microscope, Olympus; Center Valley, PA) and images collected using the Fluoview 1000 software.

4.3. Measurements of mitochondrial function

Reactive oxygen species (ROS), mitochondrial membrane potential (ΔΨm), mitochondrial calcium ($[Ca^{2+}]$m) levels and ATP production were measured in untreated controls and H2O2-treated RPE cybrids. For all flow cytometry measurements 10,000 cells were analyzed per sample.

4.4. Reactive oxygen species

Levels of cellular oxidative stress were measured by the amount of ROS generated by the RPE cybrids as previously described using 2′,7′-dichlorodihydrofluorescein diacetate (H2DCFDA), an indicator of cellular ROS generation (Degli Esposti, 2002; Amer et al., 2003; He et al., 2008). Suspensions were incubated with 0.4 μM H2DCFDA (Invitrogen Molecular Probes; Eugene, OR) in DMEM containing 5% FBS at 37 °C for 30 min in the

dark. H2DCFDA-loaded samples were centrifuged briefly, resuspended in 500 μL PBS and analyzed immediately by flow cytometry (FACSCalibur; BD Bioscience; San Jose, CA) at 488 nm excitation and 530 nm emission using Cell Quest Pro software and data calculated as H_2DCFDA fluorescence intensity units (FU).

4.5. Mitochondrial membrane potential

Mitochondrial membrane potential [ΔΨ]m was measured using tetramethylrhodamine ethyl ester, perchlorate (TMRE) (Abcam; Cambridge, MA). Samples were incubated with 250 nM TMRE (diluted in 5% FBS medium) for 30 min at 37 °C in the dark. Cells were then centrifuged, resuspended in 500 μL PBS containing 0.2% BSA, analyzed immediately by flow cytometry (FACSCalibur; BD Bioscience; San Jose, CA) at 568 nm excitation wavelength and 590 nm emission wavelength using the Cell Quest Pro software, and data expressed in fluorescence units.

4.6. Mitochondrial calcium

Changes in mitochondrial calcium levels ($[Ca^{2+}]$m) were measured in the cybrids using Rhod-2/AM (Kd ~ 570 nM) (Invitrogen Molecular Probes; Eugene, OR). Samples were loaded with 1 μM rhod-2/AM and incubated at 37 °C in the dark for 30 min. Cells were centrifuged, resuspended in 500 μL PBS, analyzed immediately by flow cytometry (LSRII; BD Bioscience; San Jose; CA) at 549 nm excitation and 581 nm emission wavelengths using FACS DIVA software and data expressed in fluorescence units.

4.7. ATP assay

ATP levels were determined using CellTiter-Glo Luminescent Cell Viability Assay (Promega; Madison, WI). Cells grown in 96 well plates were exposed to 300 μM H2O2 for 0.5, 1 and 4 h. CellTiter-Glo reagent was added at equal volumes of cell culture medium present in each well. After 12 min incubation at RT, luminescence was measured within a 0.5 s integration time using a Synergy 2 Multi-Detection Microplate Reader (Biotec; Winooski, VT) and data expressed as luminescence intensity units.

4.8. IP3R inhibition/Flow cytometry

2-Aminoethoxydiphenyl borate (2-APB) (Santa Cruz Biotechnology, sc-201487) was used to inhibit the inositol 1,4,5-triphosphate receptor (IP3R). Confluent cell monolayers were trypsinized, centrifuged, resuspended in DMEM and 500 μL cell suspension dispensed into eppendorf tubes. Experimental samples were treated with 42 μM 2-APB 1 h prior to addition of 300 μM H_2O_2 for 30 min. Treated and control samples were incubated with 1 μM Rhod-2/AM (Invitrogen Molecular Probes) at 37 °C for 30 min in the dark. Cells were centrifuged, resuspended in 500 μL PBS, analyzed by flow Cytometry (LSR II; BD Bioscience; San Jose, CA) at excitation and emission wavelengths of 549 nM and 581 nM, respectively using the FACS DIVA software and data expressed in fluorescence units.

4.9. RNAseq analysis

RNA isolation, library preparation, sequencing and differential gene expression analysis (DEG) were performed as previously described (Rubin et al., 2016) [39]. Briefly, RNA

was extracted with mirVana kit reagents (Life Technologies), and samples homogenized using a bead mill homogenizer (Bullet Blender, Next Advance). The present paper used the SureSelect Strand Specific RNA Library Preparation Kit (Agilent) to prepare the cDNA libraries. This covers the entire transcriptome, which included the 40K targets. The SureSelect Strand Specific RNA Library Preparation Kit (Agilent) was used to prepare the cDNA libraries from cybrids containing mtDNA H or J (n = 3). The libraries were sequenced on an Illumina HiSeq 2500 for 50 cycles using a single-read recipe (Illumina). Quality filtered sequencing reads were aligned to the mouse reference genome (mm10) using Tophat (version 2.0.9). FPKM (Fragments Per Kilobase of Exon Per Million Fragments Mapped) values were calculated using Cufflinks Version 2.0.2 provided with the Ensembl gene annotation (release 78). The DEGseq v1.18.0 R package was used to identify differentially expressed genes (DEG) between cybrids containing haplogroups J and H mtDNA.

The RNA samples (n = 3) were pooled prior to library preparation for RNA Sequencing as this method is followed to obtain biologically averaged gene expression values and to reduce the cost. RNA Sequencing gave us a certain biologically averaged value for each gene, and gene expression was validated further using qPCR.

4.10. Quantitative real-time PCR (qPCR)

RNA was extracted according to the manufacturer's protocol by using the RNeasy MiniKit (Qiagen, Hilden, Germany) and oncolumn DNase digestion (Rnase-free DNase Set, Qiagen). RNA concentrations were determined photometrically, and 1 μg sample was reverse transcribed with Superscript II Rnase H (Invitrogen, Karlsruhe, Germany). Quantitative real-time polymerase chain reaction (qRT-PCR) was performed in a 96-well PCR plate (Applied Biosystems, Foster City, Calif., USA) by using Quantitect SYBR Green PCR mastermix (Qiagen, Hilden, Germany). Amplification conditions were: initial heating at 95 °C for 15 min, followed by 40 cycles consisting of denaturation at 95 °C for 15 s, annealing at 57 °C for 30 s, and extension at 72 °C for 30 s in an ABI PRISM 7000 (Applied Biosystems) real-time thermal cycler. Thermocycling was completed in a final volume of 25 μl. GAPDH transcripts were used as an endogenous reference control, and each sample was normalized on the basis of its GAPDH content. Experiments were performed in triplicate for each data point. All samples were run in the same experiment.

4.11. Cytokine analysis

The Affymetrix multiplex Luminex xMAP platform (Panomics; Fremont, CA) was used to obtain quantitative measurements of cytokines in medium conditioned by the RPE cybrids. Lyophilized antigen standards were used to generate standard curves according to the manufacturer's recommendation. A volume of 50 μL conditioned medium obtained from treated (300 μM H2O2 for 48 h) and control samples was added to prewashed polystyrene antibody beads for 60 min with constant shaking at 700 rpm at RT. Beads were washed by vacuum filtration and 25 μL premixed detection antibodies added to the samples for 30 min with constant shaking at RT. After washing, beads were incubated with the detection Streptavidin-PE for 30 min at RT, and data collected using the Luminex Bio-Plex instrument (Bio-Plex 200, Bio-Rad Laboratories Inc. Hercules, CA) and Luminex acquisition software,

Bioplex Manager Version 4.11 (Biorad). Relative amounts of cytokines were calculated from standard curves.

4.12. Statistical analysis

Statistical analysis was performed using Statistics Calculators Version 3.0 beta and one-way analysis of variance (ANOVA) calculator. Results are expressed as mean ± standard error of the mean (SEM). $p < 0.05$ was taken as statistically significant.

Supplementary Material

Refer to Web version on PubMed Central for supplementary material.

References

Alge-Priglinger CS, Kreutzer T, Obholzer K, Wolf A, Mempel M, Kernt M, Kampik A, Priglinger SG, 2009. Oxidative stress-mediated induction of MMP-1 and MMP-3 in human RPE cells. Investigat. Ophthalmol. Visual Sci. 50 (11), 5495–5503.

Amer J, Goldfarb A, Fibach E, 2003. Flow cytometric measurement of reactive oxygen species production by normal and thalassaemic red blood cells. Eur. J. Haematol. 70 (2), 84–90. [PubMed: 12581189]

Anderson S, Bankier AT, Barrell BG, De Bruijn MH, Coulson AR, Drouin J, et al. , 1981. Sequence and organization of the human mitochondrial genome. Nature 290, 457–465. [PubMed: 7219534]

Balaban RS, Nemoto S, Finkel T, 2005. Mitochondria, oxidants and aging. Cell 120 (4), 483–495. [PubMed: 15734681]

Bezprozvanny I, 2011. Role of inositol 1, 4, 5-trishosphate receptors in pathogenesis of Huntington's disease and spinocerebellar ataxias. Neurochem. Res. 36 (7), 1186–1197. [PubMed: 21210219]

Boldogh IR, Pon LA, 2006. Interactions of mitochondria with the actin cytoskeleton. Biochim. Biophys. Acta Mol. Cell Res. 1763 (5), 450–462.

Brookes PS, Yoon Y, Robotham JL, Anders MW, Sheu SS, 2004. Calcium, ATP, and ROS: a mitochondrial love-hate triangle. Am. J. Physiol. Cell Physiol. 287 (4), C817–C833. [PubMed: 15355853]

Brown MD, Sun F, Wallace DC, 1997. Clustering of Caucasian Leber hereditary optic neuropathy patients containing the 11778 or 14484 mutations on an mtDNA lineage. Am. J. Hum. Genet. 60 (2), 381. [PubMed: 9012411]

Cooper GM, 2000. The Cell: A Molecular Approach, second ed. Sinauer Associates, Sunderland (MA). Structure and Organization of Actin Filaments.

Degli Esposti M, 2002. Measuring mitochondrial reactive oxygen species. Methods 26 (4), 335–340. [PubMed: 12054924]

Egorova PA, Bezprozvanny IB, 2018. Inositol 1,4,5-trisphosphate receptors and neurodegenerative disorders. FEBS J. 285 (19), 3547–3565. [PubMed: 29253316]

Egorova P, Popugaeva E, Bezprozvanny I, 2015. Disturbed calcium signaling in spinocerebellar ataxias and Alzheimer's disease. Semin. Cell Dev. Biol. 40, 127–133. [PubMed: 25846864]

Ernster L, Schatz G, 1981. Mitochondria: a historical review. J. Cell Biol. 91 (3), 227s–55s. [PubMed: 7033239]

Fehrenbacher KL, Yang HC, Gay AC, Huckaba TM, Pon LA, 2004. Live cell imaging of mitochondrial movement along actin cables in budding yeast. Curr. Biol. 14 (22), 1996–2004. [PubMed: 15556861]

Frank S, Gaume B, Bergmann-Leitner ES, Leitner WW, Robert EG, Catez F, Smith CL, Youle RJ, 2001. The role of dynamin-related protein 1, a mediator of mitochondrial fission, in apoptosis. Dev. Cell 1 (4), 515–525. [PubMed: 11703942]

Furukawa K, Smith-Swintosky VL, Mattson MP, 1995. Evidence that actin depolymerization protects hippocampal neurons against excitotoxicity by stabilizing [Ca 2+] i. Exp. Neurol. 133 (2), 153–163. [PubMed: 7649222]

Geiger K, Howes E, Gallina M, Huang XJ, Travis GH, Sarvetnick N, 1994 May. Transgenic mice expressing IFN-gamma in the retina develop inflammation of the eye and photoreceptor loss. Invest. Ophthalmol. Vis. Sci. 35 (6), 2667–2681. [PubMed: 8188461]

Guo L, Hussain AA, Limb GA, Marshall J, 1999. Age-dependent variation in metalloproteinase activity of isolated human Bruch's membrane and choroid. Investigat. Ophthalmol. Visual Sci. 40 (11), 2676–2682.

Hamid MA, Moustafa MT, Nashine S, Costa RD, Schneider K, Atilano SR, Kuppermann BD, Kenney MC, 2021 Apr 12. Anti-VEGF drugs influence epigenetic regulation and AMD-specific molecular markers in ARPE-19 cells. Cells 10 (4), 878. 10.3390/cells10040878. [PubMed: 33921543]

He Y, Ge J, Tombran-Tink J, 2008. Mitochondrial defects and dysfunction in calcium regulation in glaucomatous trabecular meshwork cells. Investigat. Ophthalmol. Visual Sci. 49 (11), 4912–4922.

Herrnstadt C, et al. , 2002. Reduced-median-network analysis of complete mitochondrial DNA coding-region sequences for the major African, Asian, and European haplogroups. Am. J. Hum. Genet. 70, 1152–1171. [PubMed: 11938495]

Hisatsune C, Mikoshiba K, 2017. IP3 receptor mutations and brain diseases in human and rodents. J. Neurochem. 141 (6), 790–807. [PubMed: 28211945]

Hudson G, Carelli V, Spruijt L, Gerards M, Mowbray C, Achilli A, et al. , 2007. Clinical expression of Leber hereditary optic neuropathy is affected by the mitochondrial DNA–haplogroup background. Am. J. Hum. Genet. 81 (2), 228–233. [PubMed: 17668373]

Ishii M, Rohrer B, 2017 Feb 6. Bystander effects elicited by single-cell photo-oxidative blue-light stimulation in retinal pigment epithelium cell networks. Cell Death Dis. 3, 16071. 10.1038/cddiscovery.2016.71.

Jones MM, Manwaring N, Wang JJ, Rochtchina E, Mitchell P, Sue CM, 2007. Mitochondrial DNA haplogroups and age-related maculopathy. Arch. Ophthalmol. 125 (9), 1235–1240. [PubMed: 17846364]

Kaarniranta K, Uusitalo H, Blasiak J, Felszeghy S, Kannan R, Kauppinen A, Salminen A, Sinha D, Ferrington D, 2020 Nov. Mechanisms of mitochondrial dysfunction and their impact on age-related macular degeneration. Prog. Retin. Eye Res. 79, 100858 10.1016/j.preteyeres.2020.100858. Epub 2020 Apr 13. [PubMed: 32298788]

Kazuno AA, Munakata K, Nagai T, Shimozono S, Tanaka M, Yoneda M, et al. , 2006. Identification of mitochondrial DNA polymorphisms that alter mitochondrial matrix pH and intracellular calcium dynamics. PLoS Genet. 2 (8), e128. [PubMed: 16895436]

Kazuno AA, Munakata K, Tanaka M, Kato N, Kato T, 2008. Relationships between mitochondrial DNA subhaplogroups and intracellular calcium dynamics. Mitochondrion 8 (2), 164–169. [PubMed: 18226984]

Kenney MC, Chwa M, Atilano SR, Pavlis JM, Falatoonzadeh P, Ramirez C, et al. , 2013a. Mitochondrial DNA variants mediate energy production and expression levels for CFH, C3 and EFEMP1 genes: implications for age-related macular degeneration. PLoS One 8 (1), e54339. [PubMed: 23365660]

Kenney MC, Hertzog D, Chak G, Atilano SR, Khatibi N, Soe K, et al. , 2013b. Mitochondrial DNA haplogroups confer differences in risk for age-related macular degeneration: a case control study. BMC Med. Genet. 14 (1), 4. [PubMed: 23302509]

Kenney MC, Chwa M, Atilano SR, Falatoonzadeh P, Ramirez C, Malik D, et al. , 2014a. Molecular and bioenergetic differences between cells with African versus European inherited mitochondrial DNA haplogroups: implications for population susceptibility to diseases. Biochim. Biophys. Acta (BBA) - Mol. Basis Dis. 1842 (2), 208–219.

Kenney MC, Chwa M, Atilano SR, Falatoonzadeh P, Ramirez C, Malik D, Tarek M, Cáceres-del-Carpio J, Nesburn AB, Boyer DS, Kuppermann BD, Vawter M, Jazwinski SM, Miceli M, Wallace DC, Udar N, 2014b. Inherited mitochondrial DNA variants can affect complement, inflammation and apoptosis pathways: insights into mitochondrial-nuclear interactions. Hum. Mol. Genet. 23 (13), 3537–3551. [PubMed: 24584571]

Khan AH, Pierce CO, De Salvo G, Griffiths H, Nelson M, Cree AJ, Menon G, Lotery AJ, 2021 Nov 8. The effect of systemic levels of TNF-alpha and complement pathway activity on outcomes of VEGF inhibition in neovascular AMD. Eye (Lond). 10.1038/s41433-021-01824-3. Epub ahead of print.

Kim YS, Joh TH, 2012. Matrix metalloproteinases, new insights into the understanding of neurodegenerative disorders. Biomol. Therapeut. 20 (2), 133.

Kowluru RA, Chan PS, 2007. Oxidative stress and diabetic retinopathy. J. Diabetes Res. 2007.

Kvanta A, Algvere PV, Berglin L, Seregard S, 1996. Subfoveal fibrovascular membranes in age-related macular degeneration express vascular endothelial growth factor. Investigat. Ophthalmol. Visual Sci. 37 (9), 1929–1934.

Lin MT, Beal MF, 2006. Mitochondrial dysfunction and oxidative stress in neurodegenerative diseases. Nature 443 (7113), 787–795. [PubMed: 17051205]

Linnane A, Ozawa T, Marzuki S, Tanaka M, 1989. Mitochondrial DNA mutations as an important contributor to ageing and degenerative diseases. Lancet 333 (8639), 642–645.

Lustbader JW, Cirilli M, Lin C, Xu HW, Takuma K, Wang N, et al. , 2004. ABAD directly links Aß to mitochondrial toxicity in Alzheimer's Disease. Science 304 (5669), 448–452. [PubMed: 15087549]

Malik D, Hsu T, Falatoonzadeh P, et al. , 2014a. Human retinal transmitochondrial cybrids with J or H mtDNA haplogroups respond differently to ultraviolet radiation: implications for retinal diseases. PLoS One 9 (2), e99003. 10.1371/journal.pone.0099003. Published 2014 Jun 11. [PubMed: 24919117]

Malik D, Hsu T, Falatoonzadeh P, Cáceres-del-Carpio J, Tarek M, Chwa M, et al. , 2014b. Human retinal transmitochondrial cybrids with J or H mtDNA haplogroups respond differently to ultraviolet radiation: implications for retinal diseases. PLoS One 9 (6), e99003. [PubMed: 24919117]

Marshall WF, Young KD, Swaffer M, Wood E, Nurse P, Kimura A, Frankel J, Wallingford J, Walbot V, Qu X, Roeder AH, 2012. What determines cell size? BMC Biol. 10 (1), 101. [PubMed: 23241366]

McCormack JG, Denton RM, 1994. Mitochondrial Ca2+ transport and the role of intramitochondrial Ca2+ in the regulation of energy metabolism. Dev. Neurosci. 15 (3–5), 165–173.

Moore AS, Wong YC, Simpson CL, Holzbaur EL, 2016. Dynamic actin cycling through mitochondrial subpopulations locally regulates the fission-fusion balance within mitochondrial networks. Nat. Commun. 7, 12886. [PubMed: 27686185]

Morris RL, Hollenbeck PJ, 1995. Axonal transport of mitochondria along microtubules and F-actin in living vertebrate neurons. J. Cell Biol. 131 (5), 1315–1326. [PubMed: 8522592]

Mueller EE, Schaier E, Brunner SM, Eder W, Mayr JA, Egger SF, et al. , 2012. Mitochondrial haplogroups and control region polymorphisms in age-related macular degeneration: a case-control study. PLoS One 7 (2), e30874. [PubMed: 22348027]

Nagase H, Visse R, Murphy G, 2006. Structure and function of matrix metalloproteinases and TIMPs. Cardiovasc. Res. 69 (3), 562–573. [PubMed: 16405877]

Olichon A, Emorine LJ, Descoins E, Pelloquin L, Brichese L, Gas N, Guillou E, Delettre C, Valette A, Hamel CP, Ducommun B, Lenaers G, Belenguer P, 2002. The human dynamin-related protein OPA1 is anchored to the mitochondrial inner membrane facing the inter-membrane space. FEBS Lett. 523 (1–3), 171–176. [PubMed: 12123827]

Osborne NN, 2010. Mitochondria: their role in ganglion cell death and survival in primary open angle glaucoma. Exp. Eye Res. 90 (6), 750–757. [PubMed: 20359479]

Pinton P, Giorgi C, Siviero R, Zecchini E, Rizzuto R, 2008a. Calcium and apoptosis: ER-mitochondria Ca2+ transfer in the control of apoptosis. Oncogene 27 (50), 6407–6418. [PubMed: 18955969]

Pinton P, Giorgi C, Siviero R, Zecchini E, Rizzuto R, 2008 Oct 27. Calcium and apoptosis: ER-mitochondria Ca2+ transfer in the control of apoptosis. Oncogene 27 (50), 6407–6418. 10.1038/onc.2008.308. [PubMed: 18955969]

Richter C, Park JW, Ames BN, 1988. Normal oxidative damage to mitochondrial and nuclear DNA is extensive. Proc. Natl. Acad. 85 (17), 6465–6467.

Rivero F, Koppel B, Peracino B, Bozzaro S, Siegert F, Weijer CJ, Schleicher M, Albrecht R, Noegel AA, 1996. The role of the cortical cytoskeleton: F-actin crosslinking proteins protect against

osmotic stress, ensure cell size, cell shape and motility, and contribute to phagocytosis and development. J. Cell Sci. 109 (11), 2679–2691. [PubMed: 8937986]

Rizzuto R, Marchi S, Bonora M, Aguiari P, Bononi A, De Stefani D, et al. , 2009. Ca 2+ transfer from the ER to mitochondria: when, how and why. Biochim. Biophys. Acta Bioenerg. 1787 (11), 1342–1351.

Rubin A, Salzberg AC, Imamura Y, Grivitishvilli A, Tombran-Tink J, 2016. Identification of novel targets of diabetic nephropathy and PEDF peptide treatment using RNA-seq. BMC Genom. 17 (1), 936.

Santel A, Fuller MT, 2001. Control of mitochondrial morphology by a human mitofusin. J. Cell Sci. 114, 867–874. [PubMed: 11181170]

Sastre J, Pallardo FV, Viña J, 2000. Mitochondrial oxidative stress plays a key role in aging and apoptosis. IUBMB Life 49 (5), 427–435. [PubMed: 10902575]

Schapira AH, 2008. Mitochondria in the aetiology and pathogenesis of Parkinson's disease. Lancet Neurol. 7 (1), 97–109. [PubMed: 18093566]

Seddon JM, George S, Rosner B, Rifai N, 2005. Progression of age-related macular degeneration: prospective assessment of C-reactive protein, interleukin 6, and other cardiovascular biomarkers. Arch. Ophthalmol. 123 (6), 774–782. [PubMed: 15955978]

Shigenaga MK, Hagen TM, Ames BN, 1994. Oxidative damage and mitochondrial decay in aging. Proc. Natl. Acad. 91, 10771–10778.

Steinbrenner H, Steinbrenner H, Bilgic E, Steinbrenner H, Bilgic E, Alili L, Sies H, Brenneisen P, 2006a. Selenoprotein P protects endothelial cells from oxidative damage by stimulation of glutathione peroxidase expression and activity. Free Radic. Res. 40 (9), 936–943. [PubMed: 17015273]

Steinbrenner H, Alili L, Bilgic E, Sies H, Brenneisen P, 2006b. Involvement of selenoprotein P in protection of human astrocytes from oxidative damage. Free Radic. Biol. Med. 40 (9), 1513–1523. [PubMed: 16632112]

Takemoto AS, Berry MJ, Bellinger FP, 2010. Role of selenoprotein P in Alzheimer's disease. Winter Ethn. Dis. 20 (1 Suppl. 1), S1–92, 5.

Torroni A, Petrozzi M, D'Urbano L, Sellitto D, Zeviani M, Carrara F, et al. , 1997. Haplotype and phylogenetic analyses suggest that one European-specific mtDNA background plays a role in the expression of Leber hereditary optic neuropathy by increasing the penetrance of the primary mutations 11778 and 14484. Am. J. Hum. Genet. 60 (5), 1107. [PubMed: 9150158]

Touhami S, Beguier F, Augustin S, Charles-Messance H, Vignaud L, Nandrot EF, Reichman S, Forster V, Mathis T, Sahel JA, Bodaghi B, Guillonneau X, Sennlaub F, 2018 Mar 16. Chronic exposure to tumor necrosis factor alpha induces retinal pigment epithelium cell dedifferentiation. J. Neuroinflammation 15 (1), 85. 10.1186/s12974-018-1106-8. [PubMed: 29548329]

Van Oven M, Kayser M, 2009. Updated comprehensive phylogenetic tree of global human mitochondrial DNA variation. Hum. Mutat. 30, E386–E394. [PubMed: 18853457]

Wallace DC. Mitochondrial genetics: a paradigm for aging and degenerative diseases? Science. 92; 256(5057):628–632. [PubMed: 1533953]

Wallace DC, 1994. Mitochondrial DNA sequence variation in human evolution and disease. Proc. Natl. Acad. 91, 8739–8746.

Wallace DC, 2005. A mitochondrial paradigm of metabolic and degenerative diseases, aging, and cancer: a dawn for evolutionary medicine. Annu. Rev. Genet. 39, 359. [PubMed: 16285865]

Wang Y, Mattson MP, Furukawa K, 2002. Endoplasmic reticulum calcium release is modulated by actin polymerization. J. Neurochem. 82 (4), 945–952. [PubMed: 12358800]

Wilkins HM, Carl SM, Swerdlow RH, 2014. Cytoplasmic hybrid (cybrid) cell lines as a practical model for mitochondriopathies. Redox Biol. 2, 619–631. [PubMed: 25460729]

Wimmers S, Strauss O, 2007 Dec. Basal calcium entry in retinal pigment epithelial cells is mediated by TRPC channels. Invest. Ophthalmol. Vis. Sci. 48 (12), 5767–5772. 10.1167/iovs.07-0412. [PubMed: 18055830]

Wong PC, Pardo CA, Borchelt DR, Lee MK, Copeland NG, Jenkins NA, et al. , 1995. An adverse property of a familial ALS-linked SOD1 mutation causes motor neuron disease characterized by vacuolar degeneration of mitochondria. Neuron 14 (6), 1105–1116. [PubMed: 7605627]

Zarbin MA, 2004. Current concepts in the pathogenesis of age-related macular degeneration. Arch. Ophthalmol. 122 (4), 598–614. [PubMed: 15078679]

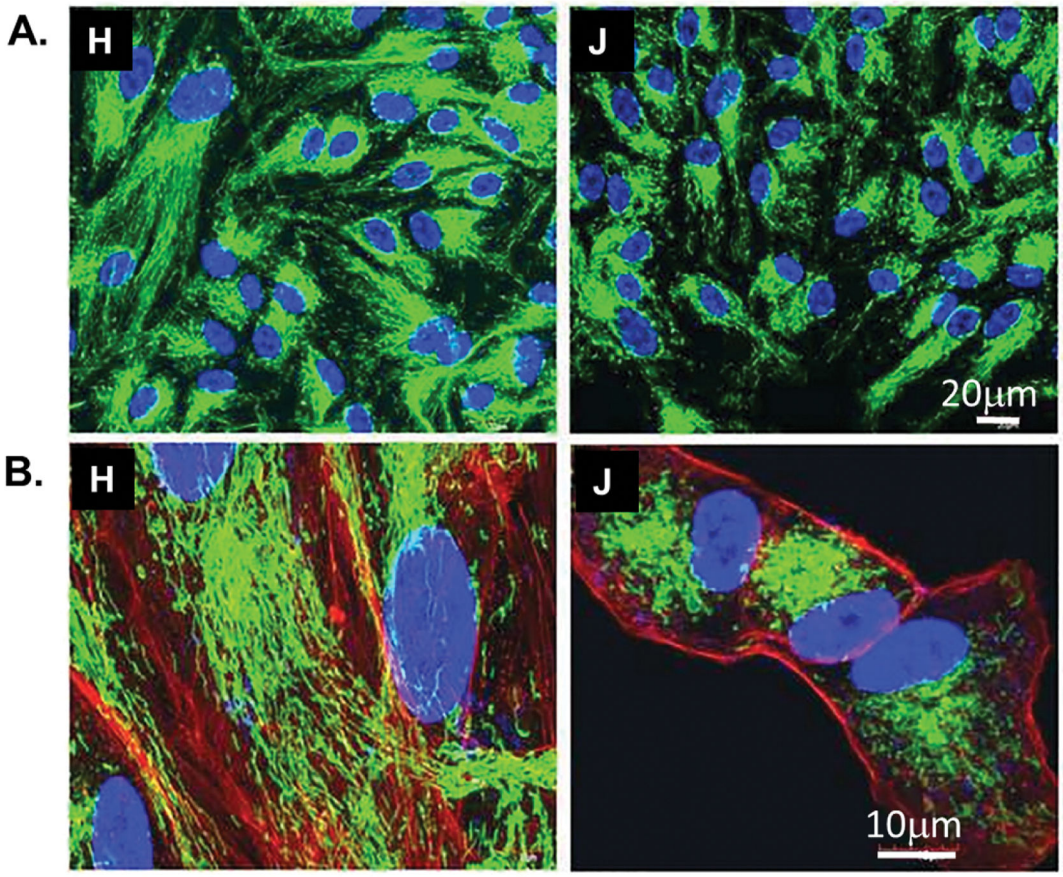

Fig. 1.

H cybrids show mt branching throughout cytoplasm; J cybrids show perinuclear **localization.** Representative image showing disruption of mitochondria and actin networks in J haplogroup mtDNA in both stressed and non-stressed conditions **A.** Mitochondria show branched networks throughout the cytoplasmic compartment in H cybrids but are seen concentrating around the nucleus in J cybrids (40x). **B.** Higher magnification shows less mitochondria branching, and actin bundles located mainly along the cell margins of J compared to H cybrids (100x). Confocal microscopy: TOMM20 (green, mt), phalloidin (red, actin), DAPI (blue, nucleus). Scale bar = 20 μM.

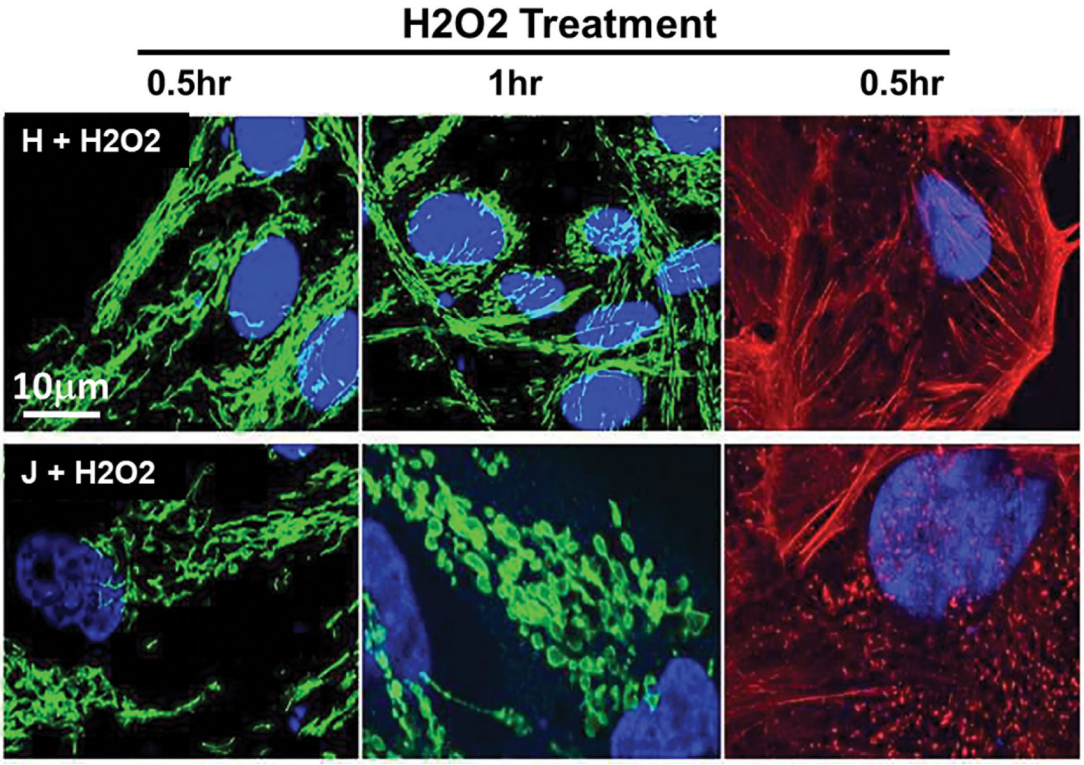

Fig. 2.

Stress induces mt fragmentation and swelling, and actin depolymerization in J **cybrids.** Representative images showing extensive mitochondrial swelling, fission and actin depolymerization in J cybrids and less so in H when the cells were exposed to oxidative stress (300 μM H2O2). H cybrids retained mitochondrial fusion and branching while J cybrids contained fragmented and swollen mitochondria with increased oxidative stress time (1 h). Actin depolymerization was evident in J and not H cybrids after short exposure to stress (0.5 h). Confocal microscopy (100x): TOMM20 (green, mt), phalloidin (red, actin), DAPI (blue, nucleus).

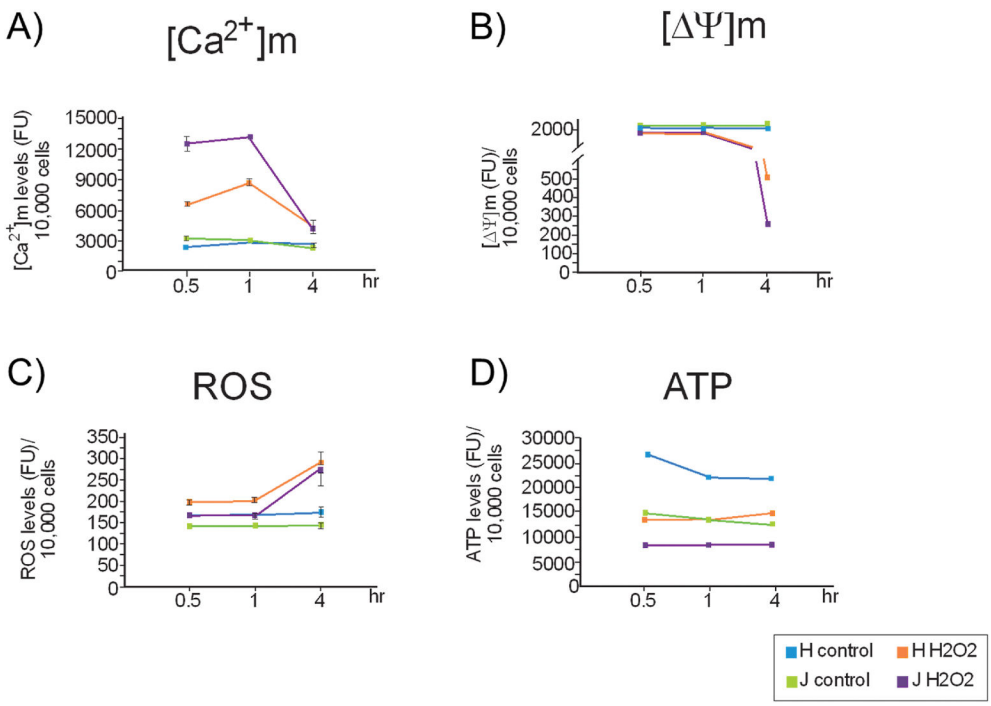

Fig. 3. H and J cybrids show differences in [Ca2+]m, (ΔΨ)m, ROS and ATP levels.

Flow cytometry results comparing mitochondrial function in H and J cybrids in non-stressed cultures and after exposure to oxidative stress. **A.** Calcium uptake by the mitochondria ($[Ca^{2+}]m$) was 50% higher in J vs H cybrids in non-stressed conditions, and $[Ca^{2+}]m$ influx was further increased after exposure to oxidative stress with maximal uptake evident by 1 h of stress. **B.** Mitochondrial membrane potential (ΔΨ)m was similar in both cybrids in non-stressed conditions, but membrane depolarization was rapid after 1 h exposure to oxidative stress (300 μM H2O2). **C, D.** Levels of both reactive oxygen species (ROS) and ATP were higher in non-stressed cultures of H compared to J cybrids by 1.2- and 1.8-fold change, respectively and remained at relatively higher levels even under 4 h of stress by 1.1 and 1.8, respectively. Non-stressed cultures: H- blue, J-green; Stress cultures: H-orange, J-pink ($n = 6$; $p \leq 0.05$).

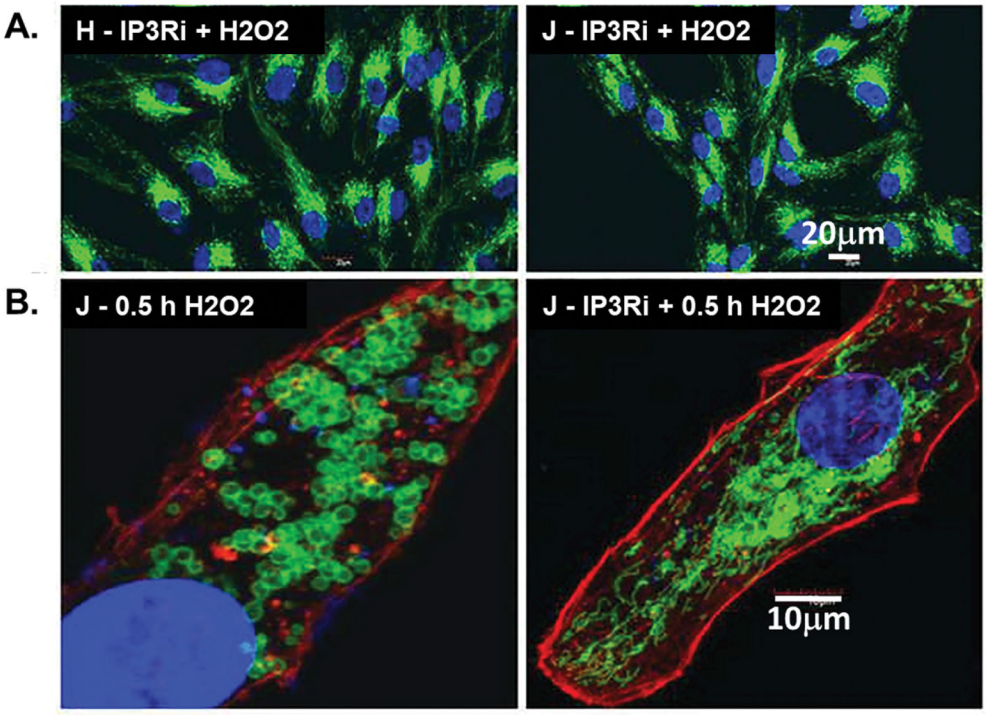

Fig. 4. Inhibition of IP3R prevented mitochondrial fragmentation and swelling in J cybrids.

A. J and H cybrids pre-treated with an IP3R inhibitor, images show improved mitochondrial network and cellular distribution in J cybrids after 30 min of oxidative stress (20x). Scale bar = 10 μM. **B.** Higher magnification images (100x) show the structural changes before and after IP3Ri in stressed condition. (green: TOMM20; red: actin; blue: dapi; n = 6). Scale bar = 20 μM.

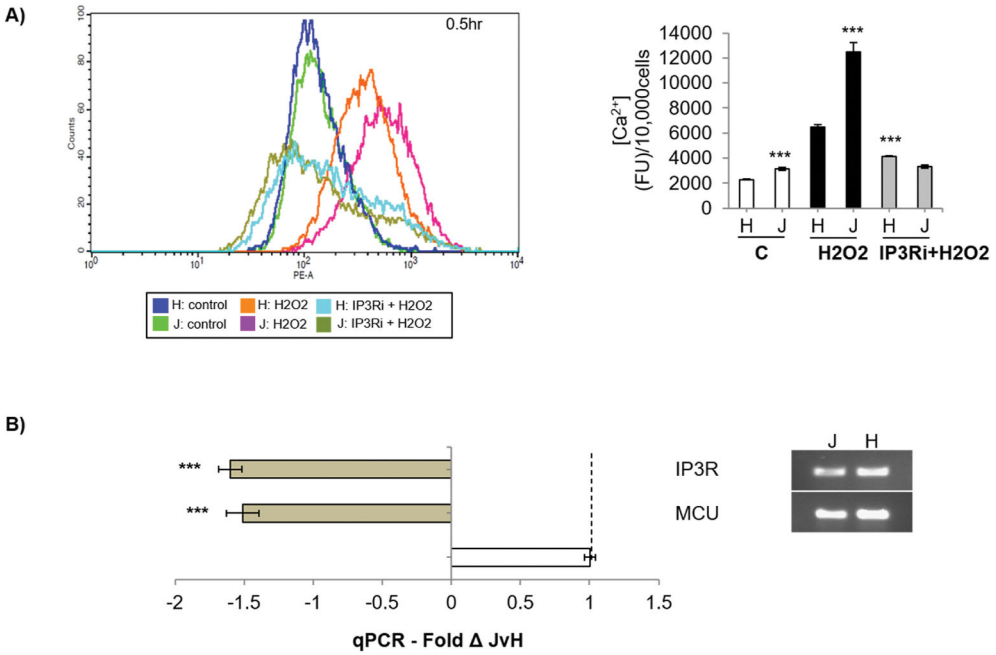

Fig. 5. Inhibition of the inositol 1,4,5-triphosphate receptor (IP3R) reduced the [Ca2+]m influx in J cybrids.

A. The flow cytometry data showed that treatment with the IP3R inhibitor, 2-Aminoethoxydiphenyl borate (2APB) decreased $[Ca^{2+}]$m under stressed conditions by 3.74-fold (n = 6; $p < 0.001$) in J cybrids as well as in H cybrids with 1.57-fold changes (n = 6; $p < 0.001$). **B.** Both RT and q-PCR showed that levels of expression of IP3R and MCU, which play a role in $[Ca^{2+}]$m, are decreased by 1.60 and 1.51-fold (n = 3; p value; H is set at 1; ***$p < 0.001$). The brown bars show negative regulation, and the white bars show positive regulation.

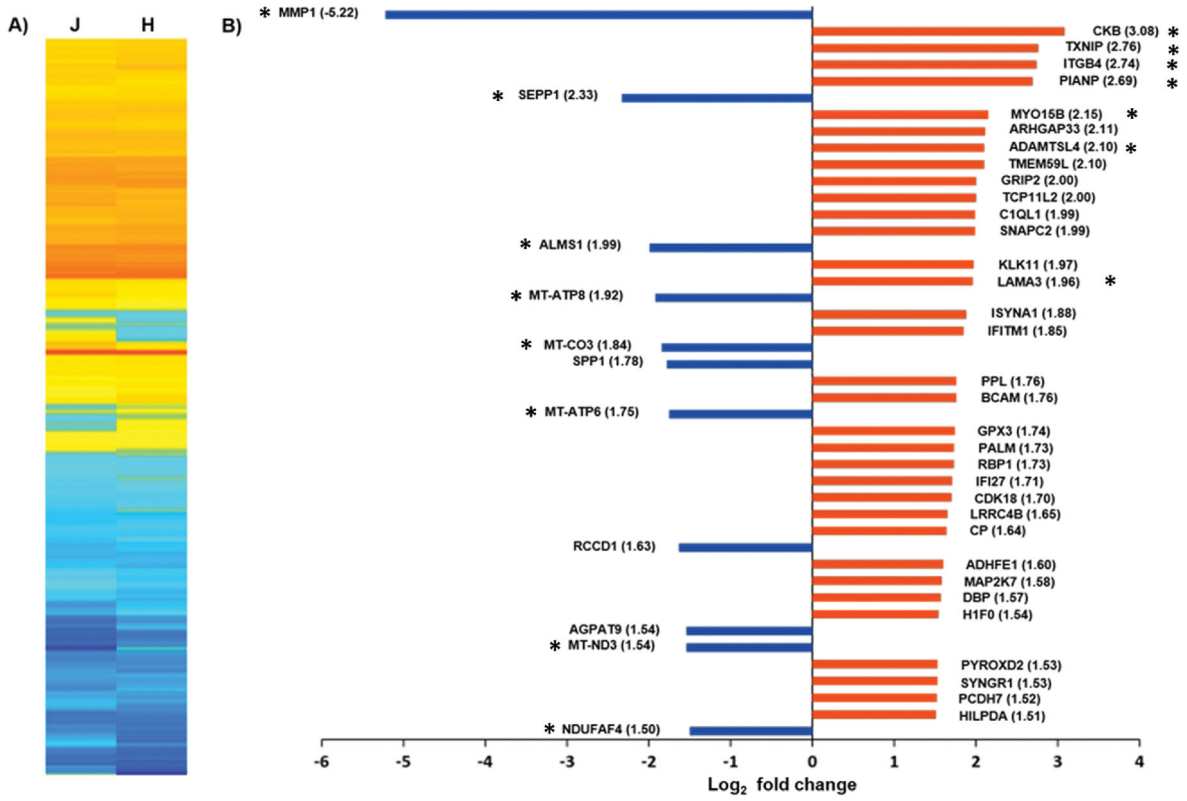

Fig. 6. J and H cybrids show transcriptome differences.

RNAseq results showing the top differentially expressed gene differences between J and H cybrids with >log2 fold changes. **A.** Heatmap depicting Z scaled RNA-Seq FPKM values of all reliably expressed genes. **B.** The horizontal graph represents the top group of genes showing >1.5 log2 changes in expression of protein-coding sequences detected by RNA-seq. Many of these represent nuclear and mitochondrial genes involved in mitochondrial function. (blue bars: downregulated; orange bars: upregulated; relative to gene expression in H cybrids; $p \leq 0.05$). The genes marked with asterisk in Fig. 6 were validated using qPCR in Fig. 7.

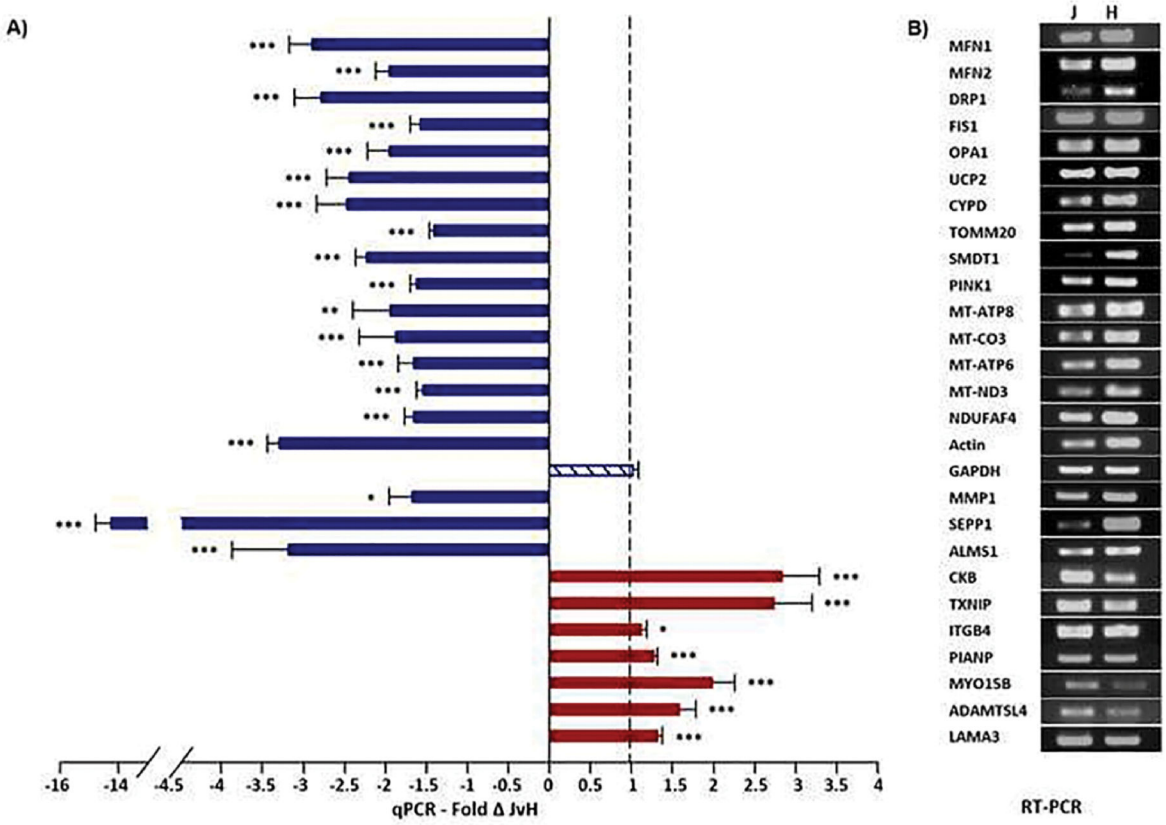

Fig. 7. Several mt genes are downregulated in J cybrids.

A select group of genes related to mitochondrial function and oxidative stress showing differential expression by RNAseq was validated by PCR analysis. **A.** The histogram shows qPCR quantitation of the expression levels of genes of interest in J compared to H cybrids. **B.** The corresponding RT-PCR gel electrophoresis images the same genes. (H values were set arbitrarily at 1 for comparison (dashed line). (n = 6; *p ≤ 0.05; **p ≤ 0.01; ***p ≤ 0.001).

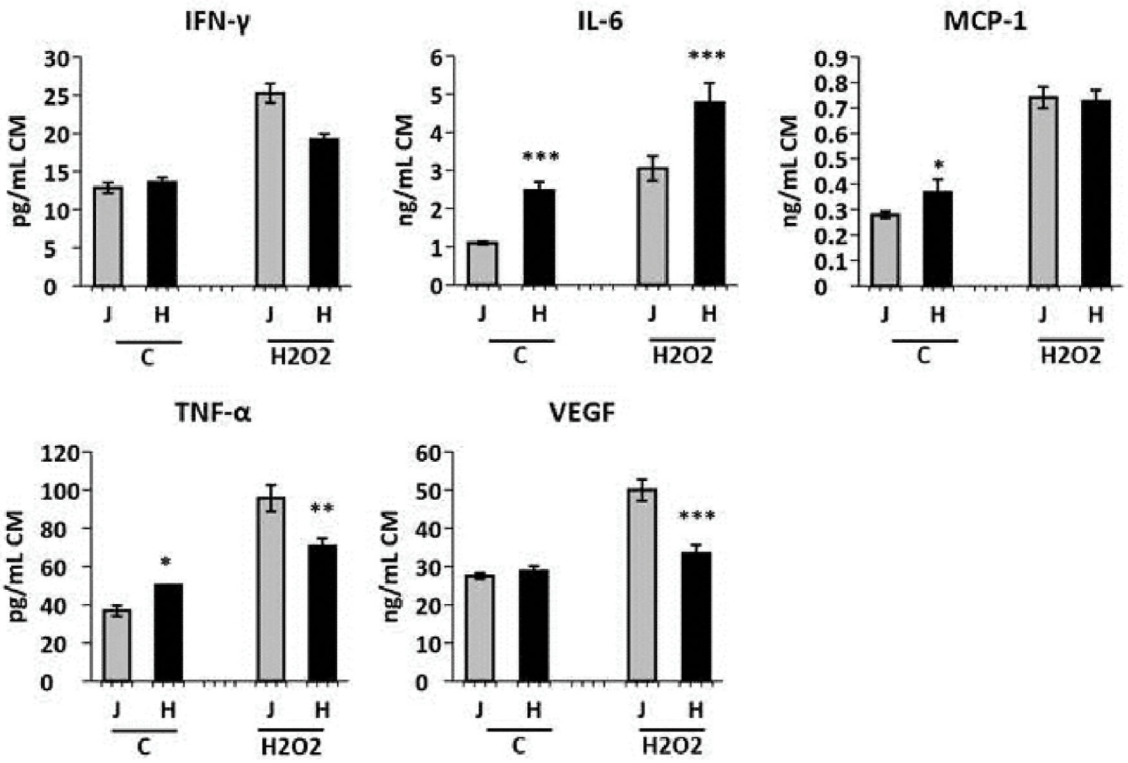

Fig. 8. J cybrids secrete more VEGF and proinflammatory cytokines than H cybrids.

J cybrids secreted significantly more TNF-α and VEGF, and less IL-6 in their media compared to H in stress conditions (300 μM H_2O_2; 48 h treatment; data given in pictograms/ml). Cytokine measurements were quantitated using Luminex beads and Bio-Plex instrument (Luminex acquisition software, Bioplex Manager Version 4.1). ($n = 6$; *$p \leq 0.05$; **$p \leq 0.01$; ***$p \leq 0.001$).